

Development and calibration of low cost MEMS IMU for UAV applications

L. Sahawneh

American University of Sharjah
Mechatronics Engineering
Sharjah, UAE
B00025029@ausharjah.edu

M.A. Jarrah

American University of Sharjah
Mechatronics Engineering
Sharjah, UAE
mjarrah@aus.edu

ABSTRACT

In this paper, an affordable and reliable low-cost Inertial Measurement Unit (IMU) is designed using commercial off-the-shelf (COTS) components. Micro Electro-Mechanical Systems (MEMS) accelerometers and rate-gyros are used, and a methodology for calibrating the resulting IMU is developed when the precise orientation of the IMU is unknown. The proposed methodology requires no precise mechanical platform for the accelerometer while a simple rotating table is utilized for the rate-gyros calibration. The proposed calibration methods utilize the fact that ideally the norm of the measured output of the accelerometer and gyro cluster is equal to the magnitude of applied force and rotational velocity, respectively. Least squares method is used to evaluate the accelerometers and gyros model coefficients.

Index Terms — IMU, COTS, MEMS

1. INTRODUCTION

The Inertial Measurement Unit (IMU) sensors calibration is one of the most challenging issues in inertial navigation. It requires high-accuracy measurements in order to maintain acceptable readings from sensors. Most of commercial low-grade IMU's have deviation of about six degrees per hour, which requires updating data every certain period of time not to lose the desired path. However advances in MEMS technology combined with minimization of electronics, have made it possible to produce chip-based inertial sensor for use in measuring angular velocity and acceleration [1].

Navigation systems are becoming standard feature of modern vehicles. On the other hand, navigation systems are crucial in designing unmanned and autonomous vehicles. Most low cost navigation systems rely on Global Positioning System (GPS) receivers as the main source of navigation information to provide the vehicle position and velocity information. However, while GPS can provide precise-long-term position information in open areas, the GPS signal could be blocked or attenuated by obstacles in urban areas resulting in GPS signal outages. In addition, low-cost GPS receivers can be easily degraded in high maneuvering environments therefore IMU/GPS integration becomes a necessary remedy to estimate position and velocity information.

In [2] a calibration procedure using optical tracking system is studied. In [3, 4] calibration procedures for the accelerometers

cluster, where the requirements of a precise control of the IMU's orientation is relaxed are proposed. These calibrations methods utilizes the fact that ideally the norm of the measured output of the accelerometer and gyro cluster should be equal to the magnitude of the applied force and rotational velocity, respectively. However, there is one major disadvantage with such a method; not all sensor parameters of the IMU are observable. This implies that these parameters (error sources) must be taken into account in the integration of the IMU with aided system, increasing the complexity of the data fusion algorithm [5].

The integration of MEMS-based inertial sensors with GPS receivers provides a system that has a superior performance in comparison with either a GPS receiver or an INS [6].

In [7] the work was done to develop an electro-mechanical system to calibrate the IMU using Global Positioning System (GPS) with four antennas. An alternate improved calibration system (Carpal Wrist) based on variable-geometry truss (VGT) was presented. The hardware part was designed for maximum pitch and roll angular and vertical displacements. Controller implementation with Cartesian kinematics has been performed with hardware response for pitch, roll, and yaw motions commanded one at a time.

Enhancing the navigation system by developing two focuses (i) implementing a tightly coupled filtering scheme to the IMU readings, and (ii) strengthening the inertial aiding of the GPS receiver tracking was proposed in [8] to build a reliable and robust aircraft to be used as a test-bed for a variety of controls experiments. The paper also discussed the physics of Dragonfly aircraft, the navigation sensors, and electronic components used in the setup. Navigation algorithms combined with GPS attitude, position and velocity measurements with the IMU's outputs to produce smoother flight condition. The algorithms were divided into distinct modules to make it easy to upgrade and test. New Kalman filter is discussed to provide smoother outputs (raw IMU delta velocities, delta angles, and raw GPS measurements of pseudo and delta range) but was not applied to the setup.

In [9] a description of an avionics system to achieve high-bandwidth feedback control, robust to modeling errors and gusts was presented. In order to have a reasonable state estimation, full state feedback suppresses undesirable cross-axis responses much better than independent SISO feedback loops, with similar closed loop bandwidth. Besides that, full state feedback was proven to

simplify system identification problem significantly. Description of all sensors used, IMU, and GPS was provided. The most complex issue in small helicopters is vibration environment. Main rotor, engine, and tail rotor are inputs which generate most of the vibrations and noises. Moreover, the suspended assembly resonances get excited by these inputs. Because of that, precise digital notch filters were used to remove those modes.

For instance, GPS derived positions have approximately white noise characteristics over the whole frequency range. The GPS-derived positions and velocities are therefore excellent external measurements for updating the INS with position parameters, thus improving its long-term accuracy. Similarly, the INS can provide precise position and velocity data for GPS signal acquisition and reacquisition after outages. In general, the fact those redundant measurements are available greatly enhances the reliability of the system [10].

Significant number of research studies have been conducted to reduce the cost of IMU unit without compromising the sensor accuracy. For example, in [11], the authors supplied the low cost sensor for the guidance, navigation, and control (GNC). The real time results of applying the low cost IMU and GPS for the (GNC) is also presented. The INS/GPS navigation loop provides continuous and reliable navigation solutions to the guidance and flight control loop for autonomous flight. With additional air data and engine thrust data, the guidance loop computes the guidance demands to follow way-point scenarios. Their real-time flight test results show that the vehicle can perform the autonomous flight reliably even under high maneuvering scenarios.

This paper describes the progress work of designing, calibrating and testing IMU unit made of commercial off-the-shelf components in the Mechatronics Center of the American university of Sharjah.

2. DESIGN SPECIFICATIONS AND SENSORS SELECTION

Inertial Measurement Unit (IMU) is the unit that responsible for inertial navigation in which it determines the pose of the vehicle through the implementation of inertial sensors; it is a six-degree of freedom inertial measurement unit consisting of three accelerometers and three orthogonal gyros to provide measurement of acceleration in three dimensions and rotation rates about three axes constructed in a “strap-down” configuration; which means that all accelerometers and gyros are fixed to a common platform and are not allowed to be controlled on gimbals; this design will eliminate the expensive moving parts mechanism required to align sensors in a pre-specified direction but instead it will require a complex mathematical computation in order to find the true vehicle position and attitude.

The selection criteria of sensors mainly based on the application that sensors utilized in, the IMU constructed from selected sensors will be a part of the avionics unit that can be implemented in a small UAV which will experience acceleration not exceeding 2g as well as the angular rotation not exceeding $\pm 150^\circ/\text{s}$. The availability and the cost of the sensors is also an important factor; besides that this reduction in cost generally brings about reduction

in reliability and accuracy. However it is our objective to use commercially available sensors in the market with the lowest cost yet acceptable quality and integrity to design an inertial navigation system that can meet UAV navigation requirements.

The accelerometers are assembled from two orthogonal low cost $\pm 2 \text{ g}$ dual axis accelerometer (ADXL202EB) [12] with high sensitivity ($12.5\%/\text{g}$) which allows the use of a lower speed counter for its PWM output. The (ADXL202EB) is a simple evaluation board that allows to quickly evaluating the performance of the ADXL202 [13] with only three additional through-hole passive components.

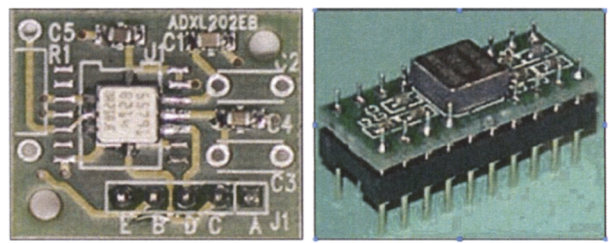


Figure 1: *ADXL202EB accelerometer evaluation board and ADXRS150EB rate-gyro.*

It provides dual axis $\pm 2 \text{ g}$ accelerometer; therefore we only need two chips to have three axis of acceleration.

In addition the manufacturer provides a behavior model (SimuLink based model), in addition we will use three orthogonal $\pm 150^\circ/\text{s}$ ADXRS150EB rate gyros [14]. The ADXRS150EB is a simple evaluation board as shown above in figure 1, which allows quickly evaluate the performance of the ADXRS150 [15] rate gyro. No additional external components are required for operation. The ADXRS150EB is still among the smallest gyros available today has a 20-lead dual-in-line (0.3 inch width by 0.1 inch pin spacing) which can be easily mounted on PCB boards.

The initial attitude of the vehicle can be estimated using a magnetometer, HMC2003 - Analog Output at 1 Volt/gauss (2.5V @ 0 gauss) - from Honeywell will be used; the sensor is shown below in figure 2. It is a high sensitive, three-axis magnetic sensor hybrid assembly used to measure low magnetic field strengths. With the sensitivity and linearity of this sensor, changes can be detected in the earth's magnetic field to provide compass headings or attitude sensing. In a later step all IMU sensor's raw measurements will be corrected, fused (i.e. using Kalman filter) and integrated to get the position and orientation of the vehicle, however to be able to calculate these integrations an initial condition of position and attitude must be known.

The IMU is designed to be modular which can be integrated easily into the avionics unit. This modular compact IMU design is shown in figure 3 below. A separate embedded computer introduced inside the unit in order to acquire the sensors measurements and perform the calibration calculations and output the data in the desired format.

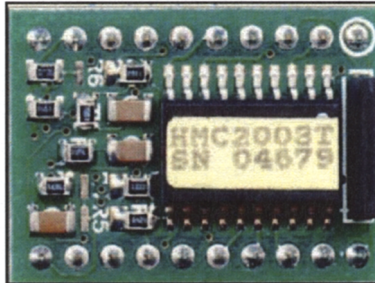


Figure 2: The Honeywell HMC2003 Magnetometer sensor.

ChipS12 (MC9S12C32) microcontroller is used as the embedded computer. It features a 16-bit HCS12 CPU, 10 bits A/D with 4.88mv resolution if $V_{ref}=5V$ used, and a large number of peripheral function blocks, such as SCI, CAN, and general-purpose-I/Os. The IMU has a separate regulated power supply circuit and it is provided with serial output peripheral so it can be easily interfaced with a PC for modifying loading the signal processing code into the microcontroller. The internal temperature of the unit is also sensed in order to provide the operation temperature inside the unit as it is an important factor affecting the sensors sensitivity or scale factor. The temperature is then used to compensate for the sensors sensitivity drifts with temperature.

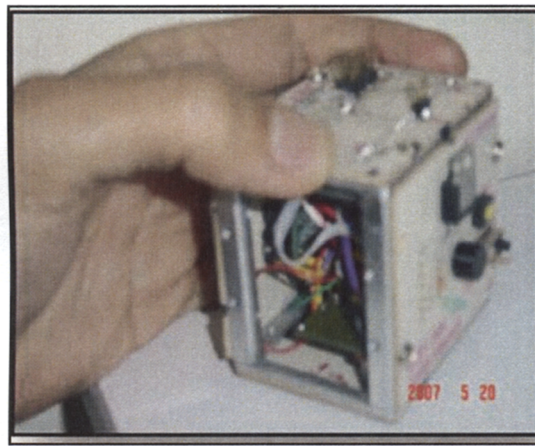


Figure 3 : The constructed (6-DOF) IMU unit, the unit dimensions are (5.9×4.6 × 5.8) cm.

2.1. Sensors Error Model

Newton's second law of motion states that the acceleration of an object is directly proportional to the magnitude of the net forces acting on the body, and inversely proportional to the mass of the object:

$$\frac{f_{net}}{m} = a = S \quad (1)$$

Where S is the specific force and a is the acceleration, which is independent on the mass. The accelerometer detects absolute accelerations due to forces applied on the body with respect

to an inertial frame. The objective is to detect the translation acceleration. Since the body force is part of the forces acting on the accelerometer mass, the equation of motion can be written as follows:

$$\begin{pmatrix} a_x \\ a_y \\ a_z \end{pmatrix} = \frac{1}{m} (f_{net} - f_{gravity}) \quad (2)$$

$$F_{trans.} = F - g \quad (3)$$

Where, a_x , a_y and a_z are the accelerations in {x, y, z} directions respectively. $F_{trans.}$ is the specific translation force, and g is the earth gravitational acceleration. In order to have an IMU of six-degrees of freedom detect accelerations and angular rates in three dimensions, two accelerometer ADXL202EB each with dual axis sensitivity are mounted so acceleration could be measured in {x, y, z} directions and three orthogonally mounted ADXRS150EB rate-gyros in order to measure angular rates $\{\omega_x \ \omega_y \ \omega_z\}$ around the accelerometer sensitive axes. Practically, the sensors are not precisely mounted orthogonally due to imperfections during the IMU construction process. Therefore, there will be a small angular position differences between inertial sensors sensitive axes and the IMU frame or platform in which inertial sensors are mounted called misalignment errors as shown in figure 4.

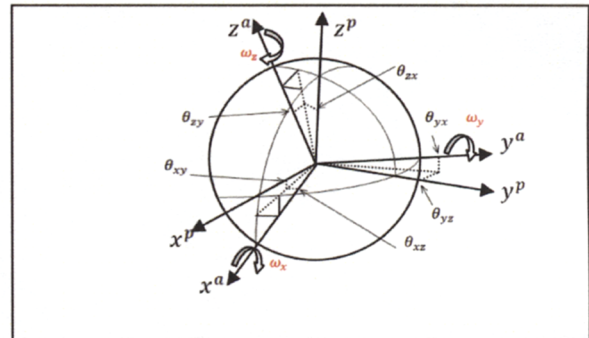


Figure 4: IMU platform coordinate axes, accelerometer and gyros sensitivity axes.

The stabilized platform (P) coordinates can be defined to be the orthogonalized accelerometer input axis coordinates or the orthogonalized accelerometer coordinates offset by a known set of three angles [4] which implies to define the transformation from the non-orthogonal accelerometer input axis cluster to the platform orthogonal coordinates with the same origin.

Because we used an ADXL202EB MEMS dual axis accelerometer to measure the acceleration in {x, y} directions, therefore, {x, y} sensitive axes could be considered as orthogonal. Defining the platform coordinates system with x-axis x^p to coincide with x^a accelerometer axis, i.e., x^p will be identical to x^a , and the y^p axis will be in the $x^a y^p$ plane with this definition the angles $\{\theta_{xz} \ \theta_{xy} \ \theta_{yx}\}$ becomes zero. Using the dot product of two unit vectors and the cosine of the misalignment angle between sensors-coordinates and the platform coordinates, the accelerometer coordinates can be estimated as follows [12]:

$$\begin{bmatrix} x^a \\ y^a \\ z^a \end{bmatrix} = \begin{bmatrix} 1 & 0 & 0 \\ \hat{y}^a \cdot \hat{x}^p & \hat{y}^a \cdot \hat{y}^p & 0 \\ \hat{z}^a \cdot \hat{x}^p & \hat{z}^a \cdot \hat{y}^p & \hat{z}^a \cdot \hat{z}^p \end{bmatrix} \begin{bmatrix} x^p \\ y^p \\ z^p \end{bmatrix} \quad (4)$$

Where x^a , y^a and z^a denotes non-orthogonal accelerometers sensitivity axis in $\{x, y, z\}$ directions respectively and x^p , y^p and z^p denotes the platform orthogonal coordinates in $\{x, y, z\}$ directions respectively. If the accelerometer axes are very nearly orthogonal or accuracy requirements are not stringent then the specific force in accelerometer coordinate axes can be transformed to a specific force estimate in platform coordinate axes assuming that the non-orthogonal sensitivity axes of the accelerometers differs by three "small" angles from the platform coordinates axes. Therefore, equation (4) can be given by the following relation[4]:

$$\begin{bmatrix} x^a \\ y^a \\ z^a \end{bmatrix} \approx \begin{bmatrix} 1 & 0 & 0 \\ \theta_{yz} & 1 & 0 \\ -\theta_{xy} & \theta_{zx} & 1 \end{bmatrix} \begin{bmatrix} x^p \\ y^p \\ z^p \end{bmatrix} \quad (5)$$

Where θ_{ij} is the rotation of i-th accelerometer sensitivity axis around j-th platform sensitivity axis.

Thus the specific force in the accelerometer cluster coordinates can be transformed into specific force estimates in platform coordinates:

$$F^p = M_a^p F^a, M_a^p \approx \begin{bmatrix} 1 & 0 & 0 \\ \theta_{yz} & 1 & 0 \\ -\theta_{xy} & \theta_{zx} & 1 \end{bmatrix} \quad (6)$$

Where M_a^p the transformation matrix between the accelerometer triad input axis and the platform coordinate.

Because the angular rates are measured using three gyros, six small rotations around the above defined platform are required to define the rotation from the gyro input axes to the platform axes. That is, three rotations are required to make the sensitivity axes of the three gyros orthogonal. Once the gyros sensitivity axes are orthogonally aligned, the direction cosine matrix needed to align the orthogonal coordinate axes with the platform coordinate axes can be obtained. Therefore the rotation in the gyros coordinate axes can be transformed into rotation in the platform coordinates as [4]:

$$\omega^p = M_g^p \omega^G, M_g^p = \begin{bmatrix} 1 & -\varphi_{yz} & \varphi_{zy} \\ \varphi_{xz} & 1 & -\varphi_{zx} \\ \varphi_{xy} & \varphi_{yx} & 1 \end{bmatrix} \quad (7)$$

And this may equivalently be written as:

$$\omega^p = R_o^p M_G^o \omega^G, M_G^o = \begin{bmatrix} 1 & -\varphi_{yz} & \varphi_{zy} \\ 0 & 1 & -\varphi_{zx} \\ 0 & 0 & 1 \end{bmatrix} \quad (8)$$

Where φ_{ij} is the rotation of i-th gyros sensitivity axis around j-th platform sensitivity axis. The matrix M_G^o transforms the non-orthogonal gyro sensitivity axes into a set of orthogonal coordinate axes and R_o^p is the direction cosine matrix transforming the gyros rates in the orthogonal sensitivity axes into platform coordinates.

The measurement errors of inertial sensors are dependent on the physical operational principle of the sensor itself. The error components include:

- 1) Internal misalignment of the sensor's input axis.
- 2) The scale factor and the scale factor linearity can then be determined by comparing the output of the gyro/accelerometer to the rotation rate/acceleration input.
- 3) Accelerometer and rate gyro biases which are the non-zero output while sensor is in the stationary status that is there is no force acting onto the sensor.
- 4) Linear acceleration sensitivity which affects the gyros stability output; i.e. for the used MEMS the linear acceleration sensitivity effect for any axis is in the order of 0.2 °/s/g.

Other errors which also play a significant role in the stability of the output of low cost inertial sensors are:

- 1) Temperature drift and nonlinearities: The better the sensor, the smaller the bias variation over the temperature range; furthermore, the better the sensor the greater the linearity of this bias variation [16]. For the MEMS sensors used in our study the temperature drift is $\pm 0.5\%$ and 5mv for accelerometer and gyros respectively and the nonlinearity is in the order of 0.2% and 0.1% of FS of a best fit to a straight line for accelerometer and gyros respectively [13,15].
- 2) Hysteresis effect: It is common for most inertial sensors. The drift rates and accelerometer biases tend to change each time the unit is switched on. This is due to the fact that measurements are noisy, and when random noise is filtered which typically most of systems used before measurements are processed and used in navigation equations that will produce what is called a random walk. The integration of this random walk will result in velocity and positions moving at different rates during different runs even the IMU (and vehicle) are in the same direction and experiencing the same acceleration during each run [17].

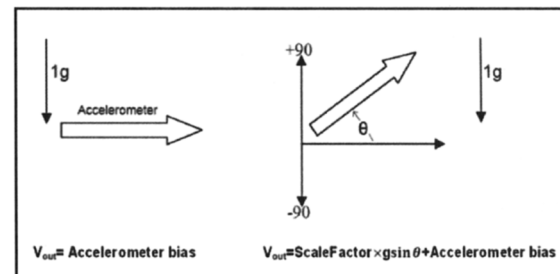


Figure 5: Accelerometer output voltage.

The measured output of a single accelerometer as shown in figure (5) can be given as:

$$D_{out} = S_{fa} \times g \sin \theta + b_a \quad (9)$$

Where D_{out} is the accelerometer output duty cycle (refer to ADXL202EB data sheet), $S_f a$ is the scale factor, g is the gravity acceleration, $(g \sin \theta)$ is the specific force along the accelerometer sensitive axis and b_a is the accelerometer nonzero bias output even though there is no component of specific force acting along the input axis. Therefore the specific force of the accelerometer x, y or z-sensitive axis is given by:

$$g \sin \theta = \frac{D_{out} - b_a}{S_f a} \Rightarrow F_o^a = \frac{D_{out} - b_a}{S_f a}. \quad (10)$$

Therefore the orthogonalized computed specific force in the platform coordinates F^p is equal to the actual measured force value in the accelerometer cluster F^a , pre-multiplied by an adopted scale factor S_a which is in turn is pre-multiplied by the non-orthogonal transformation matrix M_a^p from the accelerometer to the platform which may be modeled as [4]:

$$F^p = M_a^p S_a F^a \quad (11)$$

In an expand form (10) becomes:

$$\begin{bmatrix} F_x^p \\ F_y^p \\ F_z^p \end{bmatrix} = \begin{bmatrix} 1 & 0 & 0 \\ \theta_{yz} & 1 & 0 \\ -\theta_{xy} & \theta_{zx} & 1 \end{bmatrix} \begin{bmatrix} S_{xa} & 0 & 0 \\ 0 & S_{ya} & 0 \\ 0 & 0 & S_{za} \end{bmatrix} \begin{bmatrix} F_x^a \\ F_y^a \\ F_z^a \end{bmatrix} \quad (12)$$

Where F^p is the measured specific force vector of accelerometers, S_a the accelerometer scale factor matrix, b_a is the bias vector and v_a is a random noise on the sensor signal.

The expression for the F^a is derived by considering the actual specific force in the accelerometer coordinates to be equal to the actual output specific force pre-multiplied by the actual scale factor S_a , the actual output of an accelerometer during calibration is not equal to the actual value of apparent gravity g_a^a at calibration site. When there is no component of specific force along the input axis, there is usually a small nonzero bias output b_a . Also, allowance must be made for scale factor nonlinearity S_{anl} because accelerometer calibration coefficients vary as a function of products of components of the specific force [4].

Therefore the actual specific force measurement of the accelerometer cluster becomes:

$$S_a F^a = F_o^a + b_a + S_{anl} F_i^a F_i^a \quad (13)$$

Where $F_o^a = [F_{ox}^a \ F_{oy}^a \ F_{oz}^a]^T$ the actual raw output of accelerometers in accelerometer is input axis coordinates and: $b_a = [b_{ax} \ b_{ay} \ b_{az}]^T$, $S_a = \text{diag}[\underline{S}_{ax} \ \underline{S}_{ay} \ \underline{S}_{az}]$, $F_i^a F_i^a = [F_{ox}^2 \ F_{oy}^2 \ F_{oz}^2]^T$ and $S_{anl} = \text{diag}[S_{axnl} \ S_{aynl} \ S_{aznl}]$.

Solving Eq. (13) for F^a and combining the result with Eq. (11) yields to the following accelerometer observation equation:

$$F^p = M_a^p S_a (\underline{S}_a)^{-1} (F_o^a + b_a + S_{anl} F_i^a F_i^a) \quad (14)$$

The above model could be applied to the gyros; the measured output of the gyros may be modeled as:

$$\omega^p = M_G^p S_G (\underline{S}_G)^{-1} (\omega_o^G + b_G) \quad (15)$$

Where ω^p is the true rotational rate with respect to the inertial frame of reference, ω_o^G is the actual measured angular rate in gyro coordinates, M_G^p is the non-orthogonal transformation from gyro to platform coordinates, $S_G = \text{diag}[\underline{S}_{Gx} \ \underline{S}_{Gy} \ \underline{S}_{Gz}]$ is the adopted scale factor matrix, and $\underline{S}_G = \text{diag}[\underline{S}_{Gx} \ \underline{S}_{Gy} \ \underline{S}_{Gz}]$ is the actual scale factor matrix and $b_G = [b_{Gx} \ b_{Gy} \ b_{Gz}]^T$ is the rates bias vector.

The actual measured angular rate for each gyro can be given as:

$$V_{out} = S_f \times \omega_{oi}^G + b_G \quad (16)$$

Using the opposite sense then we can get:

$$\omega_{oi}^G = (V_{out} - b_g) / S_{fg} \quad (17)$$

Where V_{out} the gyro analog output voltage, ω_o^G is the angular rate acting along the gyros input sensitive axis; $i=x, y$ and z , S_{fg} is the gyro scale factor and b_g is the gyros nonzero bias output.

3. CALIBRATION PROCEDURE AND EXPERIMENT SETUP

Modern calibration procedures utilize the benefits of Kalman filtering to obtain optimal estimates of the calibration coefficients. Obtaining analytical results for calibrations based on Kalman filtering is extremely difficult. However, analytical results can be derived for inverse and least-squares solutions of the calibration observation equations [4]. However, calibration is usually performed in the field for platform-mounted inertial instruments at the factory for body-mounted instruments, with the advent of GPS; the factory calibrations for body-mounted instruments can be updated to a degree during navigation [4].

Traditionally, a mechanical platform rotating the IMU into different precisely controlled orientations and angular rates has been used to calibrate IMU's. Then, observing the output and the pre-calculated specific force or angular velocity input acting upon the IMU for different orientations and rotation sequences, respectively it is straightforward to estimate the misalignment, scaling and bias [4, 18, 19]. The cost of such platform often exceeds the cost of developing and constructing a MEMS sensor based IMU. Therefore, a calibration procedure is desirable where the requirements of a precisely controlled orientation of the IMU can be relaxed [5].

The sensors are calibrated by comparing the analogue (ADXRS150EB-rategyro) or digital signals (ADXL202EB-accelerometer) produced by the sensor, with known input motion. Thus, from the rate transfer tests, the output signals from a gyroscope can be compared with the accurately known rotation rate and scale-factor defined as so many millivolts per degree per second of rotation rate, for instance. Similarly, using the gravity vector as an accurate standard, the scale-factor of an accelerometer can be defined. There are several different levels at which error compensation can be applied. However, the fundamental idea is the same for all; to correct the effects of a

predictable systematic error, or errors, on the accuracy of a sensor. Additionally, a basic requirement is that an error process can be estimated using identification methods and that a signal corresponding to the disturbing effect, such as temperature or acceleration, is available and can be measured to the required accuracy [17].

Predictable error components can be used in the opposite sense to correct, or compensate; often this technique relies on the use of a constant coefficient in the error representation, but for more demanding applications, or complex error behavior, it is common to use polynomial representations.

The accuracy that may be achieved from the application of compensation techniques is dependent on precisely how the coefficients in the error equation represent the actual sensor errors. This representation can often vary as a function of time, the environment in which the sensor is used, and how often it is used. For the more demanding applications, it may require to recalibrate the sensor regularly, to ensure that the compensation routines are as effective as required by the particular application.

The method of calibration described here is for platform-mounted instruments and is based on performing a series of instrument cluster rotations from one orientation to the next. The constructed IMU is fixed on a platform consisting of a Dividing Head Semi Universal table [20] which is manually rotated. The platform accuracy is $\pm 0.5^\circ$. The residuals are observed for a period of time at each orientation, after completing the series of observations, the data are used to compute the calibrations coefficients. The sensors outputs are sampled by 16-bit acquisition card at sampling time = 0.0002 sec using real-time Dspace® hardware. Data sets are saved and processed using Matlab® then the sampled voltage signals are converted to angular rate and specific force using a Simulink® model. The Simulink® model is an implementation of Eq. 10 and Eq.16. Performing a separate test, coefficients (scale factor and bias) of accelerometers and gyros are calibrated individually, i.e., the relationship between the sensor output voltage (duty- cycle or analog output voltage) and the physical quantity acting along the sensor sensitivity axis is modeled. The calibration process is based on performing a series of instrument cluster manual rotations from -90° to +90° with a step of 5° along each accelerometer sensor sensitivity axis and a series of angular rotations starting from -150°/sec to 150°/sec with a step of 30°/sec along each gyro sensor sensitivity axis. Data sets (1000 samples/each observation using real-time Dspace®) are observed from 38 different static orientations and 11 rotations for each accelerometer and gyro respectively.

The “Curve Fitting Toolbox” in Matlab® is used to estimate each accelerometer and gyro coefficients. Results are shown in figures 6, 7 and 8 and summarized in table 1. Generally the calibration rotation is designed to provide measurement residuals that, together as a whole, reflect the effect of all of accelerometer and gyro calibration coefficients.

During the accelerometer calibration, the specific force output is compared to the computed apparent gravity obtained from a gravity survey through the calibration rotation schedule. Any difference is used to calculate accelerometer calibration coefficient values that force the computed specific force to agree with the extrapolated gravity value. The comparison is made by

means of observation equations which were derived earlier (eq. 14) and then using least square method to determine the accelerometer calibration coefficients. Note that there are 12 unknowns in the observation equation. An 18-static observation schedule is designed. Each accelerometer input axis is placed in an up and down orientation and at all possible halfway in between orientations as [4]. The measurement residual for each observation is $(g_a^p - S_o^a)$. It is the best to use the measurement residual composed of the magnitude of the apparent gravity vector at the calibration side minus the magnitude of the accelerometer triad. Using the magnitude difference obviates the necessity to precisely control the platform orientation during the calibration rotations [4]. The data sets collected from the 18-different static orientations at a constant temperature (25°C) and a general least squares algorithm is applied to the data to estimate accelerometer observation coefficients.

The least squares function for the accelerometer calibration as defined by [4] is:

$$X_a \beta_a = Y_a \quad (16)$$

Where:

$\beta_a = [\theta_{zx} \theta_{xy} \theta_{yz} b_{ax} b_{ay} b_{az} \delta \hat{S}_{ax} \delta \hat{S}_{ay} \delta \hat{S}_{az} S_{axn} S_{ayn} S_{azn}]^T$ is the estimated coefficient vector and $\delta \hat{S}_{ai} = \delta \hat{S}_{ax}/S_{ai}$ is the normalized scale factor perturbation, in which the scale factor perturbation is the difference between the actual and nominal values:

$S_{ai} = S_{ai} + \delta \hat{S}_{ax}$, $i=x, y$ and z . and Y_a to be the vector of measurement residuals, X_a is the first-order Taylor series expansion coefficient matrix of accelerometer observation Eq.14. Then the calibration coefficients are evaluated [19]:

$$\beta_a = (X_a^T X_a)^{-1} X_a^T Y_a \quad (17)$$

In the same manner the sensed rotation rate of gyro cluster is compared to a reference rate, which is either the Earth rate or the sum of the rotation of the Earth and an accurately commanded rate; however using the Earth rate has two disadvantages. The Earth rotation rate is only 15°/h, and the horizontal component is small at high latitudes [4].

The orthogonalized sensed angular rate is equal to the actual measure rate, pre-multiplied by the scale factor matrix and the orthogonalized transformation from gyro platform axes. The platform axes have been defined to be the orthogonalized accelerometer axes as shown in the observation equation (eq.15). During the gyros calibration, the sensed rotation rate output is compared to the computed commanded rate obtained from a gravity survey through the calibration rotation schedule; any difference is used to calculate gyros calibration coefficient values that force the computed commanded rate to agree with the extrapolated rate survey value. The comparison is made by means of observation equations which derived earlier (eq. 15) and then using least square method to determine the gyros calibration coefficients. Note that there are 12 unknowns in the observation equation. An 18 observation schedule is designed. The measurement residual for each observation is $(\omega_r^p - \omega_o^G)$; it is the best to use

the measurement residual composed of the magnitude of the reference rate vector at the calibration side minus the magnitude of the gyro triad.

The least squares function for the gyros calibration as defined by [4] is:

$$X_G \beta_G = Y_G \quad (16)$$

Where:

$\beta_G = [\varphi_{xz} \varphi_{yz} \varphi_{zy} \varphi_{xy} \varphi_{yx} \varphi_{zx} b_{Gx} b_{Gy} b_{Gz} \delta\hat{s}_{Gx} \delta\hat{s}_{Gy} \delta\hat{s}_{Gz}]$ is the estimated coefficient vector and $\delta\hat{s}_{Gi} = \delta S_{Gi}/S_{Gi}$ is the normalized scale factor perturbation, in which the scale factor perturbation is the difference between the actual and nominal values:

$S_{Gi} = S_{Gi} + \delta\hat{s}_{Gi}$, $i=x, y$ and z . and Y_G to be the vector of measurement residuals, X_G is the first-order Taylor series expansion coefficient matrix of gyro observation Eq.15. Then the calibration coefficients are evaluated [21]:

$$\beta_G = (X_G^T X_G)^{-1} X_G^T Y_G \quad (18)$$

4. RESULTS

4.1 Accelerometer Calibration and Identification results:

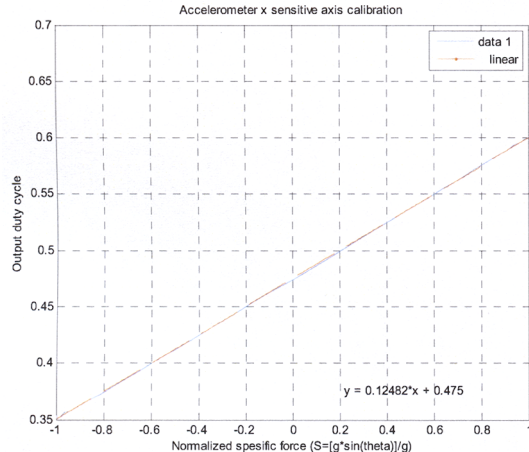


Figure 6: Output Duty Cycle versus normalized specific force acting along accelerometer sensitivity x-axis.

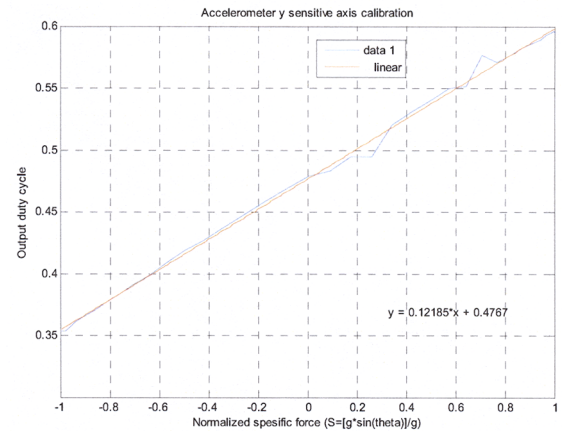


Figure 7: Output Duty Cycle versus normalized specific force acting along accelerometer sensitivity y-axis.

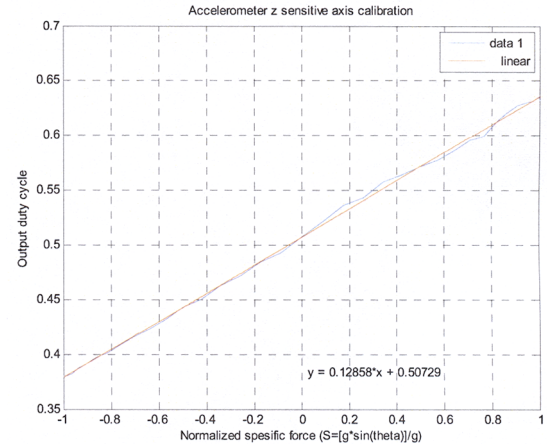


Figure 8: Output Duty Cycle versus normalized specific force acting along accelerometer sensitivity z-axis.

Table 1: Accelerometers estimated scale factor and biases ($V_{out} = S_f \times g \sin \theta + b_a$). The platform was manually positioned into 38 different orientations, at each orientation the sensor's outputs were sampled by 16-bit acquisition card at sampling time of 0.0001 sec for a period of 1 sec using real-time Dspace®.

Axis	Scaling (S_f)	Bias (b_a) (Duty Cycle %)
x	0.12482	0.47500 (47.500 %)
y	0.12185	0.47670 (47.670 %)
Z	0.12858	0.50729 (50.729 %)

Table 2: IMU results, Accelerometers triad observation equation coefficients using least squares estimate.

Axis	Scaling	Bias(m/s ²)	Axis	Misalignment
x	-0.0032	-0.0350	θ_{zx}	-0.0199
y	0.0003	0.3976	θ_{xy}	0.0941
z	-0.0789	0.7783	θ_{yz}	-0.0201
Axis Nonlinearity scaling				
x	-0.0037			
y	-0.0165			
z	-0.1545			

4.2 Gyros Calibration and Identification results:

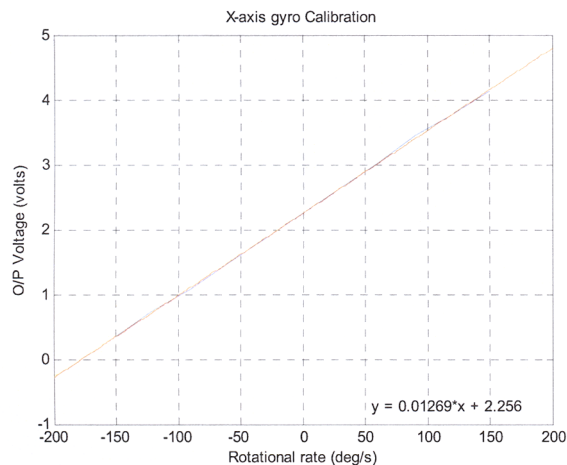


Figure 9 Output voltage versus commanded rotational rate acting along gyros sensitivity x-axis.

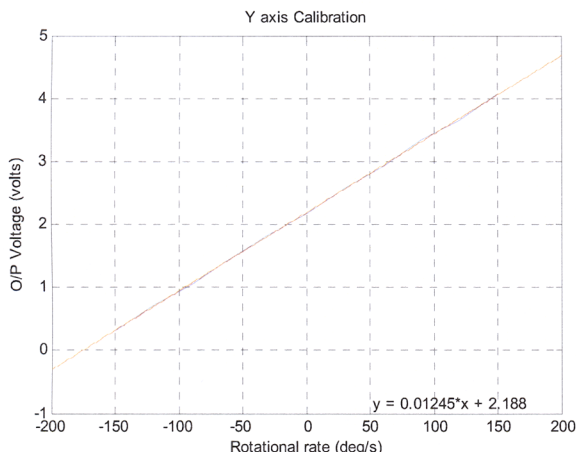


Figure 10 Output voltage versus commanded rotational rate acting along gyros sensitivity y-axis.

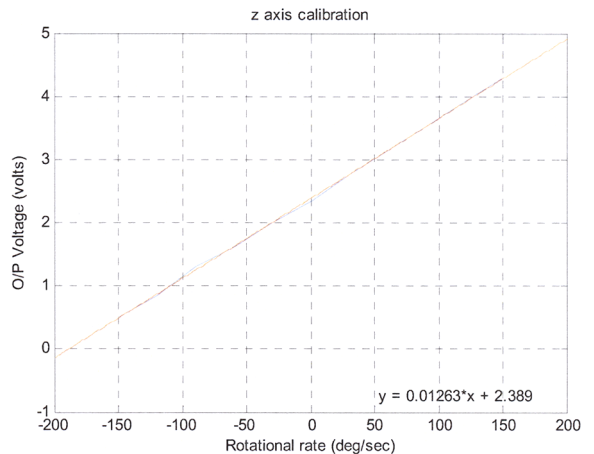


Figure 11 Output voltage versus commanded rotational rate acting along gyros sensitivity z-axis.

Table 3: Gyros estimated scale factor and biases ($V_{out} = S_f \times \omega + b_g$). Data was collected from 11 rotations, at each orientation the sensor's output voltages were sampled by 16-bit acquisition card at sampling time of 0.0001 sec for a period of 1 sec using real-time Dspace®.

Axis	Scaling (S_f)	Bias (b_g) (volts)
x	0.01269	2.256
y	0.01245	2.188
Z	0.01263	2.389

Table 4: IMU results, gyros triad observation equation coefficients using least squares estimate.

Axis	Scaling	Bias (%/s)	Axis	Misalignment
x	0.0107	0.3658	φ_{xz}	-0.0294
y	0.0078	1.3338	φ_{yz}	0.0369
z	0.0300	3.4827	φ_{zy}	0.0252
Axis Misalignment				
φ_{xy}	0.0174			
φ_{yx}	0.0398			
φ_{zx}	0.0117			

5. CONCLUSIONS

We envision that in the future, that building a compact low cost IMU unit that will be integrated in an Avionics unit ready to be implemented within the designed AUS-UAV. GPS integration with Kalman filter for sensor readings tuning is proposed to the next phase and future work in progress of producing the AUS-UAV complete setup. Still not all the gyros sensor model coefficients are studied such as the specific force dependent gyro coefficients. However, the proposed method can be considered

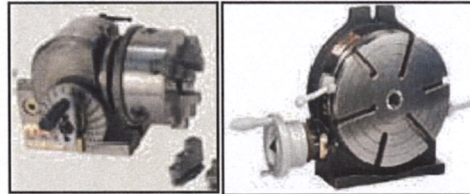
useful for many low-cost applications where the cost of constructing a mechanical platform many times exceeds the cost of developing the inertial measurement unit.

6. ACKNOWLEDGEMENT

I wish to acknowledge the assistance of Eng. H. Sadjadi and Eng. A. Al radaideh, through the design, and manufacturing processes, as well as I would like to thank my current job boss Mr. K. Kaabar for his encouragement and support.

REFERENCES

- [1] Schelling, R. (1999). "A Low-Cost Angular Rate Sensor for Automotive Applications in Surface Micromachining Technology", Third Annual International Conference on Advanced Microsystems for Automotive Applications Proceedings, March 1999.
- [2] A. Kim and M.F Golnaraghi "Initial calibration of an inertial measurement unit using an optical position tracking system", in Proc. PLANS 2004, IEEE Position Location and Navigation Symposium, 26–29 April. 2004, pp. 96 – 101.
- [3] Z.C. Wu, Z.F. Wang and Y. Ge, "Gravity based online calibration of monolithic tri-axial accelerometers' gain and offset drift.", in Proc.4-th World Congress on Intelligent Control and Automation., 10–14 June. 2002.
- [4] A. Chatfield, "Fundamentals of High Accuracy Inertial Navigation," American Institute of Aeronautics and Astronautics (AIAA), volume 174, 1997.
- [5] I. Skog, P. Handel, 'Calibration of MEMS Inertial Measurement Unit", XVII IMEKO WORLD CONGRESS, Metrology for a Sustainable Development. September, 17–22, 2006 Rio de Janeiro, Brazil.
- [6] Niu X. and El-Sheimy N. "The Development of a Low-cost MEMS IMU/GPS Navigation System for Land Vehicles Using Auxiliary Velocity Updates in the Body Frame", Mobile Multi-Sensor Systems Research Group, The University of Calgary.
- [7] Hall J., Williams II R., Graas F., Ohio University, "Cartesian Control for the Inertial Measurement Unit Calibration Platform", ASME Design Technical Conferences, Baltimore, MD, September 2000.
- [8] Evans J., Hodge W., Liebman J., Tomlin C., Parkinson B. "Flight Test of an Unmanned Air Vehicle with Integrated Multi-Antenna GPS Receiver and IMU: Towards a Testbed for Distributed Control and Formation Flight", Proceedings of the ION-GPS Conference, Nashville, September 1999.
- [9] Gavrilets V., Shterenberg A., Dahleh M. A., Feron E. "Avionics System for a Small Unmanned Helicopter Performing Aggressive maneuvers", M.I.T., Cambridge, MA.
- [10] El-Sheimy, N. (2000): "An Expert Knowledge GPS/INS System for Mobile Mapping and GIS Applications", Proceeding of the 2000 National Technical Meeting of the Satellite Division of the Institute of Navigation – January 26-28, 2000, California, USA.
- [11] Jong- Hyak k., Stuart Wishart, Sukkarieh S., "Real-time Navigation, Guidance, and Control of a UAV using Low-Cost Sensors"2006, University Of Sydney.
- [12] [1ADXL202EB Dual Axis Accelerometer Evaluation Board Data Sheet (REV. A), 1995-2008 Analog Devices Inc. <http://www.analog.com>.
- [13] ADXL202/210 data sheet, 1995-2008 Analog Devices Inc. <http://www.analog.com>.
- [14] ADXRS150EB 150 /s Single Chip Rate Gyro Evaluation Board, 1995-2008, Analog Devices Inc. <http://www.analog.com>.
- [15] ADXRS150 data sheet, 1995-2008 Analog Devices Inc. <http://www.analog.com>.
- [16] Nebot, E., and Durrant-Whyte, H., "Initial calibration and Alignment of Low-Cost Inertial Navigation for Land Vehicle Applications," Journal of Robotics Systems, Vol.16, No. 2, February, 1999, pp. 81-92.
- [17] Titterton, D., Weston, J., "Strapdown Inertial Navigation Technology," 2nd Edition (2004: IEE).
- [18] R M. Rogers, Applied Mathematics In integrated Navigation Systems, Second Edition. AIAA Education Series, 2003.
- [19] J.C. Hung, J.R. Thacher and H.V. White, "Calibration of accelerometer triad of an IMU with drifting Z -accelerometer bias", in Proc. NAECON 1989, IEEE Aerospace and Electronics Conference, 22–26 May. 1989, vol. 1, pp. 153 – 158.
- [20] " Excel Dividing Heads Semi Universal" and "HV6 (2-200-100) Excel Precision Rotary Tables", <http://www.excelmachinetools.co.uk/accessories/14/dividing-heads-rotary-tables/74/index.html>.



- [21] Montgomery, D., Runger, G., "Applied Statistics and Probability for Engineers," Second Edition, 1999.